Proceedings of
11th European Conference on Turbomachinery Fluid dynamics & Thermodynamics
ETC11, March 23-27, 2015, Madrid, Spain

RESPONSE OF A TRANSONIC COMPRESSOR TO A MASSIVE INLET DISTORTION

F. Wartzek - C. Brandstetter - F. Holzinger - H.-P. Schiffer

Technische Universität Darmstadt
Institute of Gas Turbines and Aerospace Propulsion
Otto-Berndt-Straße 2, 64287 Darmstadt, Germany

ABSTRACT

The demand to extend the flight envelope of an aircraft makes predicting the behaviour of a plane and its components close to its aerodynamic limits imperative. The interaction of the plane, the engine and the atmosphere is still challenging to model. One problem is that by reducing the stability margin the risk of disturbances rises. A separation in the intake can lead to a distortion of the inflow, especially for the engines. In contrast to academic experiments, this publication shows the investigation of a realistic distortion pattern in a transonic compressor stage. A bevelled beam was installed upstream of the rotor. The radial extent was 10% of the channel height, the circumferential extent was 120°. This beam generated a separation that extended into the rotor. The interaction of this massive separation with the compressor was investigated using high-resolution measurement techniques. The flow in the compressor was influenced around the entire circumference and span even though the distortion was located only at the casing.

NOMENCLATURE

SC	Smooth casing without distortion
NS	Near stall (last stable operating point)
PE	Peak efficiency of smooth casing
DG	Distortion generator
N100	100% design speed
N65	65% design speed
p_s	static pressure
$\overline{p_s}$	ensemble averaged static pressure
π_t	Total pressure ratio
π_s	Static pressure relative to total inlet pressure
σ_{rel}	Relative standard deviation (standard deviation divided by mean)
FHP	Five Hole Probe
Ma	Mach number

INTRODUCTION

Flying is a transport that is extremely dependent on weather conditions. Strong gusts, heavy rain or snow often lead to cancellation of flights. The number of passengers per year is increasing, leading to more flight traffic. Acceptance that the weather can prevent flying is low. The risk is a possible stall of the wing or the engine due to the interaction of the aircraft with the atmosphere. A stability margin is needed to ensure safe operation of all components across the entire operation range. Additionally, flight manoeuvres are planned to become more severe, for example, the increasing angle of attack of the aircraft. A steeper angle during landing or take-off reduces perceived noise on the ground and reduces flight time. Consequently the influence of the weather must be reduced and the flight envelope extended. To do this, either the stability limit has to be expanded or the stability margin

decreased. This increases the risk of flow disturbances as all components are operated closer to their aerodynamic limits.

To solve this problem, researchers try to predict the reaction of the aircraft and the engine to flow disturbances as well as their formation. For a modern aircraft, atmospheric turbulences, such as gusts, are only modelled roughly and only considered by an increased safety margin. Interaction of components, like intake, wing and engine, is usually neglected. Numerical simulation of an entire aircraft close to its limits in interaction with a simulation of atmospheric turbulence is still too challenging. The DFG[1] research group "FOR1066 - Simulation of Wing and Nacelle Stall" is working on a methodology that will increase the accuracy of these simulations. For an overview of their work see Radespiel et al. [June 2013] and Niehuis et al. [September 2013].

Common practise for the design of an engine nacelle is to ignore the compressor system. The nacelle's stalling point is simulated with undistorted inflow and as a through-flow model. In reality, a typical nacelle inflow distortion pattern is a longitudinal vortex, for example, the ground vortex (Mishra et al. [December 2011] and Shmilovich and Yadlin [June 2006]). Another source of inflow disturbances is separations. Colin et al. [2007] and Hall and Hynes [2006] show a large separated area in the intake and the appearance of an additional inlet vortex. Numerically, the biggest challenge is the combination of two problems: the complex flow in separations and in turbo-machines. Accurate prediction of the separation point and the reattachment of the flow is extremely dependent on the numerical model. For turbo-machines, the problem is the combination of complex geometries with compressible flow, high levels of turbulence and unsteadiness.

A further problem is the missing circumferential periodicity. Full 360° setups or advanced numerical models (like the Non-Linear-Harmonic method) are necessary. In the inflow and the compressor, none of the passages is exposed to the same flow, therefore, no periodic boundary conditions can be defined. This leads to a drastic increase in computation times per operating point.

Today, experimental investigations are the most promising way to gain insights into these flows. Screens are the state-of-the-art for generating disturbances in engine experiments (e.g. Gunn et al. [June 2013] and Lin et al. [June 2005]). However, screens generate a homogeneous total pressure drop that is not comparable to realistic inflow distortion patterns. They are highly inhomogeneous in space and time, as shown by Davis et al. [April 2002]. However, pressure fields generated by screens are easier to generate and measure.

During an initial measurement campaign, the hardware was designed to integrate distortion bodies into the test section. An overview of the results is given by Lieser et al. [September 2011]. A more detailed view of the data and concluding remarks are given by Wartzek et al. [2012].

This publication shows the experimental investigation of a more realistic inflow distortion pattern. The direct interaction of a separation bubble with a transonic compressor stage was investigated. This separation bubble is representative of a stalled engine nacelle.

EXPERIMENTAL SETUP

The measurements presented in this paper were performed at the single stage Darmstadt Transonic Compressor. The rig is operated by the Institute of Gas Turbines and Aerospace Propulsion at the Technische Universität Darmstadt.

Test Rig Key technical parameters of the test rig and the investigated stage are summarized in Table 1. For the tests, the "Rotor 1 - Stator 2" configuration was used. More details of the rig design and the stage can be found in Schulze et al. [1995]; Müller [2011] shows previous results of the stage. Figure 1 shows a sketch of the test rig. The rig is operated in an open-loop configuration. Air is sucked in from the left and guided to the settling chamber. In the settling chamber, the inlet conditions are

[1] German research foundation

measured. The air flows through a nozzle into the test section. Downstream of the stage the air passes the throttle and the exit diffuser and is guided to ambience. The compressor is driven by a DC-drive that is connected to a gear box. A torquemeter measures speed and torque as work input for efficiency calculation.

max. power	800 kW
max. torque	350 Nm
design mass flow	16 $^{kg}/_{s}$
design speed	20,000 rpm
outer diameter	0.38 m
hub-to-tip-ratio	0.51
rotor blades	16
stator blades	29

Table 1: Key parameters of the Darmstadt Transonic Compressor

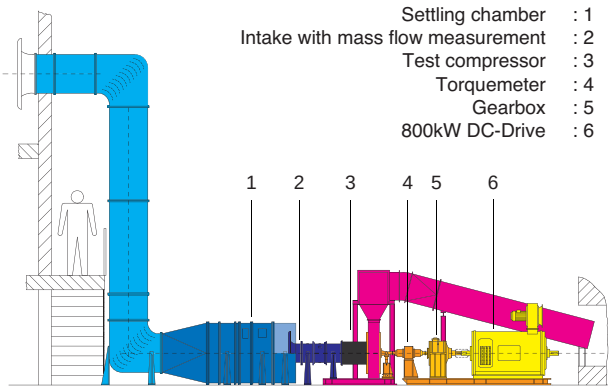

Figure 1: Sketch of the Darmstadt Transonic Compressor

Distortion In an engine intake separation occurs due to a change in the angle of attack of the inflow without additional solid flow blockage. Due to the constraints of the rig, inclining the intake was not possible. Therefore, the separation was generated by a step in the flow. A beam was inserted into the test section with a radial extent of 10% of the inlet channel height and a circumferential extent of 120°. The beam is shown in green in Figure 2.

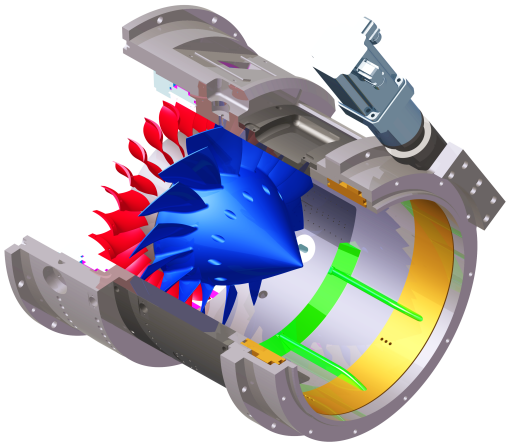

(a) Figure of the casing with Rotor, Stator and Distortion

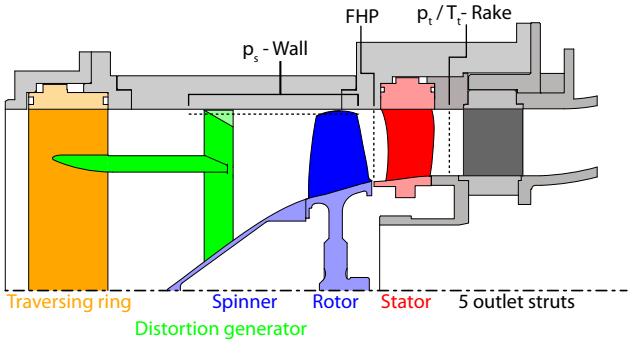

(b) Sketch of the measurement positions and the configuration

Figure 2: Measurement Setup

Based on the results obtained in the first campaign (see Wartzek et al. [2012]) it was decided to cover more than 60° of the circumference. For a single distorted sector Longley and Greitzer [1992] reported that the angle has to be greater than 90° to get the maximum effect. As shown by Colin et al. [2007] or Hall and Hynes [2006] the extent of a separation in a realistic intake can even reach up to angles of 180°. Still the identification of a representative separation is difficult as usually only through flow models are investigated. The design intent of the used beam was to produce a significant separation near the blade tip to get a massive tip flow distortion. This is of special interest as from former measurement campaigns (see Bergner et al. [2006]), the rotor is known to be tip-critical. The

radial extent of the beam was therefore fixed to be 20% of the blade height. Nevertheless detailed data of the flow structures inside a realistic separation, in front of a fan, are not available. The data presented here can be used to validate numerical models. With these validated models realistic geometries and stalling engine configurations can then be simulated.

To suppress a possible separation on the upstream side, the beam was bevelled with an angle of 30°. The distortion generator (DG) was connected to a traversing ring (shown in yellow). To enable the integration of measurement techniques, the traversing ring was located upstream the rotor. The beam was connected to the ring by three supports. The distance to the blade tip leading edge was two axial blade chord lengths. Due to the relative movement of DG and casing, a radial gap of 1 mm was necessary.

Instrumentation The flow structures caused by the distortion and their missing periodicity demand greater measuring effort compared to classic circumferential symmetric configurations. A 360° traverse is necessary to capture the influence of the DG. Different types of steady and time-resolving measuring techniques were used. In Figure 2b the measurement positions are shown. The exit plane of the stage is measured with two total pressure and two total temperature rakes. These rakes are used to calculate the total pressure ratio and the performance of the stage. Each of the rakes is equipped with eleven radial measuring positions.

The total pressure at rotor exit was measured with a Five Hole Probe (FHP). For the flow upstream of the rotor, pressure taps, measuring the static wall pressure, were installed. Unsteady information on the flow was measured using an array of pressure transducers flush mounted into the casing wall. KULITE XCS-062 were used as transducers. The data was recorded using SPECTRUM 16 bit A/D-Boards, with a maximum sampling frequency of 500 kHz.

Measuring Procedure For improved accessibility and to ease the integration, the instrumentation is fixed in the casing. Different relative positions are achieved by traversing the stator or the DG. The performance of the whole compressor is calculated by assuming periodicity of this measured flow field. The distortion caused a non-periodic flow field, which extended around the circumference. As explained previously, it is not possible to assume periodic conditions for any part of the circumference; therefore the DG had to be traversed 360°. As both stator and DG could be traversed, all clocking positions between them could be achieved. Finally, 290 circumferential positions were measured for the exit instrumentation and the wall pressure taps. The time for a performance measurement was significantly higher than for SC. Two points on two speed lines were measured. The measured points for both configurations are shown in Figure 4, with the 100% design speed line (N100) as a transonic characteristic and the 65% design speed line (N65) as a subsonic characteristic. For the DG configuration, the mass flow for peak efficiency is not determinable as only two operating points were measured. With DG, the first operating point is the peak efficiency point for the SC configuration (PE). At both speeds the compressor was throttled until it stalled. The last stable operating point (near stall - NS) was identified and measured individually for SC and DG.

In this paper the results for N100 are analysed in detail. The subsonic operating points show more or less the same effects. Though with reduced amplitudes and without the shock-related phenomena. More details on the comparison of both speeds can be found in Wartzek et al. [2014].

RESULTS

The measurements are presented and analysed in this section. The DG configuration is compared to SC. First, a model for the stage flow is show. Starting with the global behaviour showing the overall impact of the distortion on the compressor. Then the results are presented in the direction of flow direction from upstream of the rotor to downstream of the stator.

Developed Flow Model Based on the results of the measurements a flow model was developed to simplify the understanding of the effects and their origins. This model will be presented first, then the measurements are shown in detail. The different measurement techniques and positions prove the applicability of the model. Figure 3 shows the model, representing the flow in the compressor stage when operating with an inflow distortion. Furthermore this Figure introduces the specific terms used in this paper.

The air comes in from the left; the rotor rotates from top to bottom. The side where the rotor enters the distortion will be referred to as the "entry side", the other side as the "exit side".

The separation is narrowed by the compressor as the air is sucked into the rotor. This leads to a bow of the streamlines and a swirl component is induced in the flow around the beam. On the entry side of the beam this results in co-rotating swirl, which is counter-rotating on the exit side. This swirl changes the incidence, depending on the side of the beam. For the entry side, shown with green arrows, the incidence is lowered. For the exit side, shown with red arrows, the incidence is raised. Gunn et al. [June 2013] observed similar effects in their experiments with a screen upstream of the rotor. The rotor causes a slightly asymmetric shape of the separation. Both sides are moved in the direction of rotation, leading to a more inclined angle of the "separation line shear layer" on the entry side and a steeper one on the exit side. This effect can be seen by comparing the dashed green line and the dashed red line at the edges of the beam in Figure 3. At the corners of the beam a circular corner vortex is formed. At the boundary of the separation, due to the shear layer, a loss structure appears, formed by the interaction with the main flow. At the centre of the beam a spot exists where the flow stagnates inside the separation.

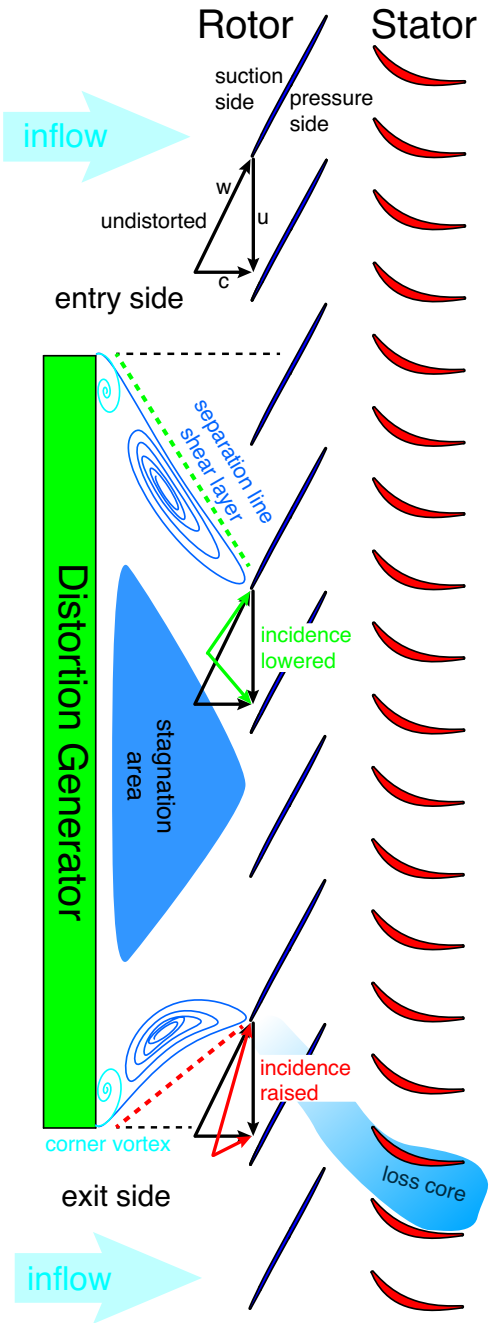

Figure 3: Sketch of flow phenomena

Global Data The compressor map for the stage is shown in Figure 4. The N100 speed line is shown in red. The dots represent the measured points, the solid line the total pressure ratio. This is calculated by dividing the area average of the total pressure downstream of the stator by the total inlet pressure from the settling chamber. The dashed line shows the efficiency, calculated using the input power from the torquemeter and the total pressure ratio. To get a better impression of the stage's behaviour the N65 speed line is shown in green.

The mass flow is referenced to ISA atmosphere[2] using the inlet conditions from the settling chamber. The squares show the results for the distorted configuration. Due to the distortion influence the total pressure in front of the rotor is lowered and the mass flow redistributed. This effect is neglected in order to show the general behaviour of the stage and the measured operating points. Nevertheless, the loss in stability margin can be seen, as indicated by the dashed lines. Even though the stalling mass flow remains the same the total pressure ratio is lowered. This leads to a loss in operating range.

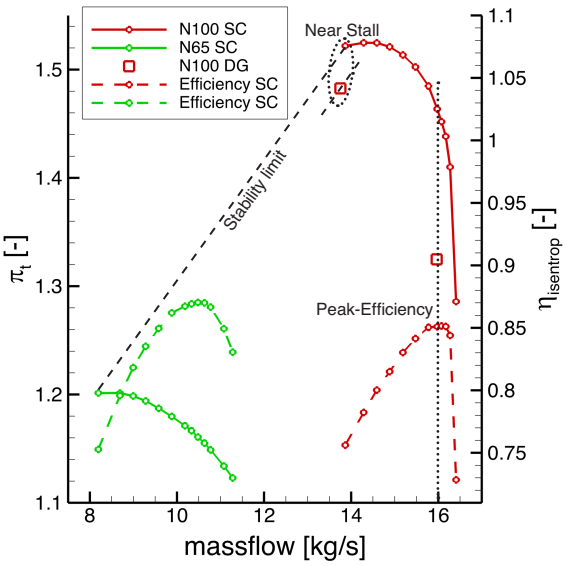

Figure 4: Compressor map of the stage

The efficiency for the distorted case is not shown as it is difficult to compare only the two points with SC. Still at NS the efficiency drops by around 1%. At PE the efficiency drops by around 10% indicating that the massflow for maximum efficiency changed. This is difficult to analyse by having only two points of the speed line. Nevertheless this drop would be relevant if such an inflow distortion appears while the rotor is operating in PE conditions, e.g. during cruise.

Upstream Rotor The steady static wall pressure is shown in Figure 5. Air comes in from the left, the rotor rotates from top to bottom. For clarification of the measurement position, one rotor blade is shown. This only shows the position of the rotor as the data is steady and therefore averaged over the blades. Figure 5a shows the PE results; Figure 5b the NS operating point.

The static pressure decreases from upstream of the DG up to the rotor leading edge as the flow is accelerated by the spinner of the rotor (see Figure 2b). Upstream of the DG the pressure increases as a result of the blockage. Immediately in front of the beam the pressure decreases again as the velocity is increased through the gap between beam and casing. This is a result of the higher pressure ratio from upstream of the DG to the separation downstream of the DG.

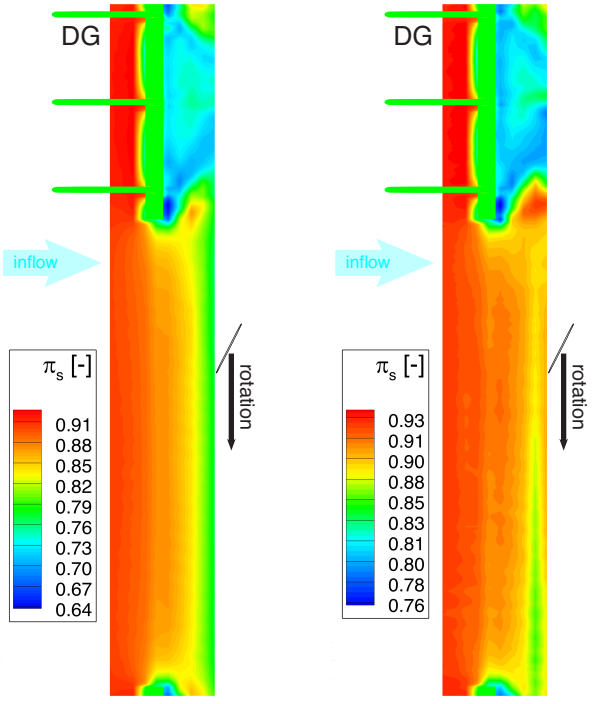

(a) PE with DG (b) NS with DG

Figure 5: Steady static wall pressure

Downstream of the DG, the separation is clearly visible in the static pressure. A drop of between 18% and 25% in static pressure, relative to the maximum pressure upstream of the beam, was caused by the DG. The pressure loss downstream of the DG and the intensity of the separation seems to be lower for NS. This is due to the reduced intensity of the separation as the velocity upstream of the DG is lower (the mass flow is reduced from PE to NS). The effects described in Figure 3 are clearly identifiable as are a stagnation area downstream of the DG, as well as the pressure drop caused by

[2]International Standard Atmosphere as defined by the International Civil Aviation Organization

the corner vortices and the separation line shear layer. The change in incidence is more difficult to recognize. An increase in pressure on the exit side can be seen.

Rotor Flow In this section the results of the time resolving pressure transducers are analysed. In Figure 6a the results for the PE operating point are shown. Figure 6b shows the results for the last stable operating point NS. As the operating points can be considered steady, the data is ensemble averaged over around 1300 revolutions. The relative static pressure is calculated by dividing the ensemble averaged pressure by the total inlet pressure. The standard deviation is calculated for the same 1300 revolutions at every position and then divided by the mean pressure to get the relative standard deviation. This amount of revolutions is sufficient, as the average value does not change when more revolutions are considered. For better comparability, the colour maps between the operating points are identical. In equation (1) the used formulas are shown.

$$\pi_s = \frac{\overline{p_s}}{p_{t,inlet}} \qquad \sigma_{rel} = \frac{1}{\overline{p_s}} \sqrt{\frac{1}{n-1} \sum_{i=1}^{n} (p_{s,i} - \overline{p_s})^2} \tag{1}$$

Taking a look at the reference data on the left in Figures 6a and 6b, typical flow features for a transonic compressor are visible. At PE a shock close to the leading edge is visible. This shock impinges the neighbouring blade in the downstream half of the suction side. An area with low pressure and increased standard deviation close to the leading edge of the suction side reveals the trajectory of the tip leakage vortex. When this vortex crosses the shock, at PE only a little interaction is recognisable. Downstream of the shock, on the suction side of the blade, the pressure decreases due to the Prandtl Meyer Expansion.

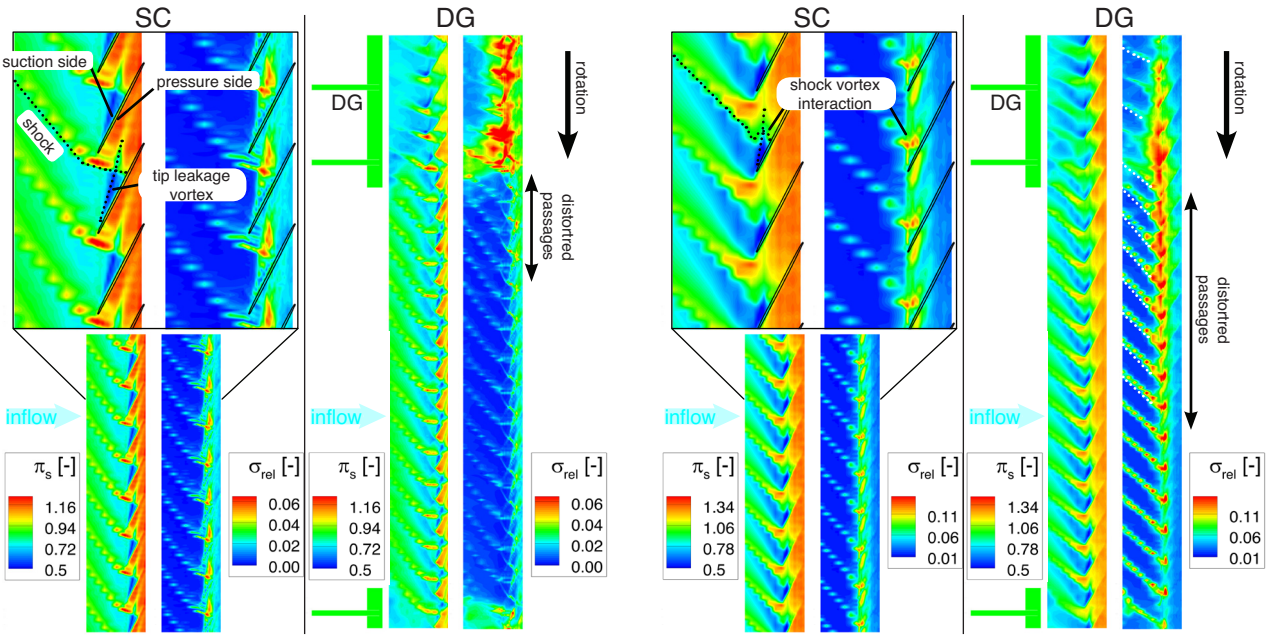

(a) PE (b) NS

Figure 6: Unsteady static wall pressure

For NS the general structures remain the same. Due to the positive incidence the pressure difference across the blade is increased. Therefore the tip leakage vortex is strengthened and its trajectory is more inclined in the circumferential direction. The shock detaches from the leading edge due to the higher backpressure. This changes the interaction of the tip leakage vortex with the shock. The shock

front is bowed where the vortex crosses the shock. The trajectory is moved further in the circumferential direction and the size of the vortex increases. More details on the tip flow structures in this stage can be found in Biela et al. [2008]. A detailed view of these structures can be found in Brandstetter et al. [September 2011].

The data for the distorted configuration on the right in Figures 6a and 6b looks completely different. The static pressure ratio downstream of the rotor is decreased compared to SC. This is reasonable, as the total pressure ratio is decreased as well (Figure 4). The pressure of the SC configuration is not restored over the whole circumference.

For PE, in Figure 6a, the structure downstream of the DG seems to be similar to the steady results in Figure 5. The corner vortex and the shear layer result in increased values of standard deviation. Inside the stagnation area, the pressure is slightly increased with low values of fluctuation. Downstream of the DG the shock system of the blades seems to disappear completely. On the exit side, the incidence is increased, as can be seen in the higher pressure values at the blade leading edge (as shown in Figure 3). The relative standard deviation is highest where the rotor interacts with the separation line shear layer at the exit side. This is the area where the loss core from Figure 3 is located. The standard deviation inside the blade passage is increased over the following three passages, in terms of rotation. The black arrow indicates this. In the remaining part of the circumference, the flow looks more or less constant. Especially in the standard deviation, the values are even lower compared to SC.

At NS (Figure 6b), this changes. Downstream of the DG the pressure is decreased only slightly compared to PE, as explained previously. The shock changes its angle while passing the separation. Inside the separation, the angle is flat and the shock is more horizontal. When the blade leaves the separation the shock strength is intensified and moves its trajectory more in a circumferential direction, indicated by the dotted lines. The local increase in incidence on the exit side is not visible anymore. Despite the stagnation pressure at the leading edge seems to increase continuously from inside the separation to the entry side of the DG. The maximum of the relative standard deviation is located on the exit side of the DG. Hence, the separation disturbs the flow over more passages compared to PE, as indicated by the longer black arrow. The standard deviation is increased around the whole circumference. This is also in contrast to PE. It seems that the impact of the separation on the rotor is much severe at NS than at PE. This could be due to the already higher blade loading and the associated higher risk of local separations on the blade.

Downstream Rotor The outflow of the rotor is measured with an FHP. As probe measurements are more time consuming than performance measurements, less positions were measured relative to the DG. These positions are not equally distributed around the circumference. Based on the static wall pressure, distinct positions were chosen. In Figure 7 these positions are shown by the black dots.

As only distinct circumferential positions were measured, a representative two-dimensional visualisation of the total pressure ratio is difficult. The flow around the circumference differs too much, so an interpolation of the values will be erroneous. Nevertheless, the identification of strong gradients is easier when the data is interpolated to a plane, especially as the distribution of the positions is not equidistant. This interpolation is shown in Figure 7.

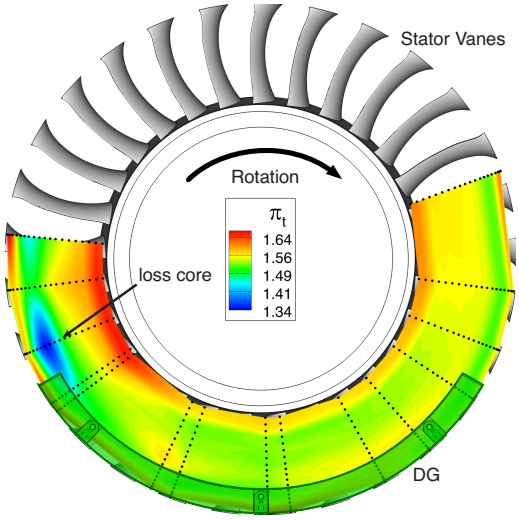

Figure 7: FHP - NS DG downstream rotor

The total pressure is normalised by the inlet total pressure in the settling chamber. This leads to an error in interpreting the work input for the DG configuration. The total pressure upstream of the rotor

is lowered by the DG. Therefore, the total pressure ratio calculated with the values from the settling chamber will be lower than the one calculated with the values immediately upstream of the rotor. As shown, the flow in the complete stage changes. The inlet total pressure loss would result only in a changed total pressure ratio in the small area immediately behind the DG. It is known from other measurements that the total pressure behind the DG decreases by 25%. Therefore, to determinate of the local work input of the rotor, the total pressure behind the DG should be used to calculate the local total pressure ratio. This would not change the results shown here.

A significant drop in total pressure appears at the exit side of the beam in the tip region. It seems that this drop in total pressure ratio is located in a small, limited area. The total pressure at the hub is, in contrast, altered. Close to the casing, the influence of this loss seems small. This explains why this loss is not so clearly visible in the rotor tip flow (Figure 6). An explanation for this loss core, as shown in figure 3, could be the interaction of the rotor with the shear layer of the separation. Possibly the raised incidence leads to a local break down of the blade flow. As described previously, the total pressure ratio at the entry side is lowered as the incidence decreases.

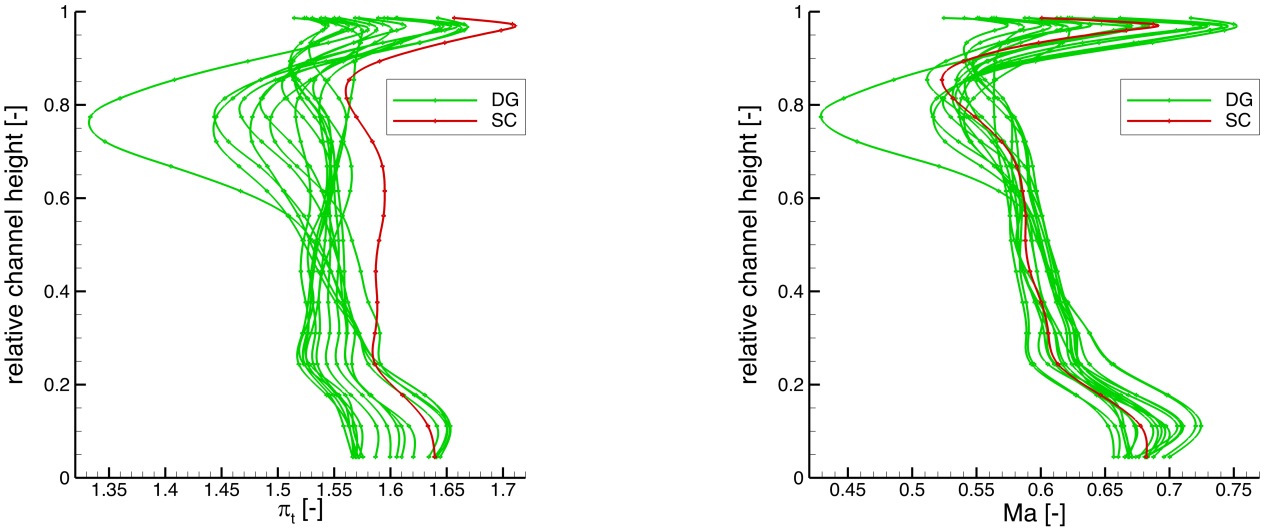

(a) Total pressure ratio downstream the rotor

(b) Ma downstream the rotor

Figure 8: Radial profiles at NS downstream rotor - from FHP (DG configuration in green, SC in red)

In Figure 8, the radial profiles of the FHP are compared with SC. In Figure 8a the total pressure profiles, as used for the two dimensional visualisation, are shown. In the upper 75% of the channel, the DG configuration builds up less total pressure for all measurement positions. Below 25% of the channel, a few profiles show an increased total pressure level. These areas can be seen in Figure 7 as well.

Looking at the Mach number distribution, the results are more consistent with the reference data. The level of the flow Mach number is in the same dimension as the reference. The distribution of the Mach number is typical for an NS operating point with a maximum at the tip.

This further supports the theory that, while driving the compressor at the reference's mass flow, the work input of the rotor is lowered for the whole circumference and radius. The spread of the lines and shapes is in agreement with the results from the rotor tip in Figure 6. The compressor operates at different conditions around the whole circumference. Only one position stands out, as a local reduction in velocity and total pressure ratio is significantly visible at around 80% height. This position is the same as the one marked in Figure 7. The loss core from Figure 3 leads to a reduction in pressure ratio and velocity.

As the stability limit is the more interesting operating point for a compressor stage only these results are shown. Still it can be stated, that the explained behaviour is even more pronounced for

PE. Except the loss core that can be seen at the stability limit is not present. As already visible in the performance map (Fig. 4) the difference in the operating points is much bigger for PE. Therefore the difference between PE and SC in the total pressure ratio is bigger as well. At PE the pressure ratio of SC is not restored for any of the measurement positions. The Mach number differs consequently more as well. This could be an indicator that the operating point with DG is not the point of maximum efficiency anymore. Hence, the overall rotor behaviour is not really comparable. Still it gives an impression of the impact of an inflow distortion on a rotor when operated at PE.

Downstream Stator The total pressure at stage outflow is shown in figure 9. For better visualisation in Figures 9a and 9b the data of the measured stator passage for the SC configuration were multiplied. The total pressure is again normalised by the inlet total pressure in the settling chamber.

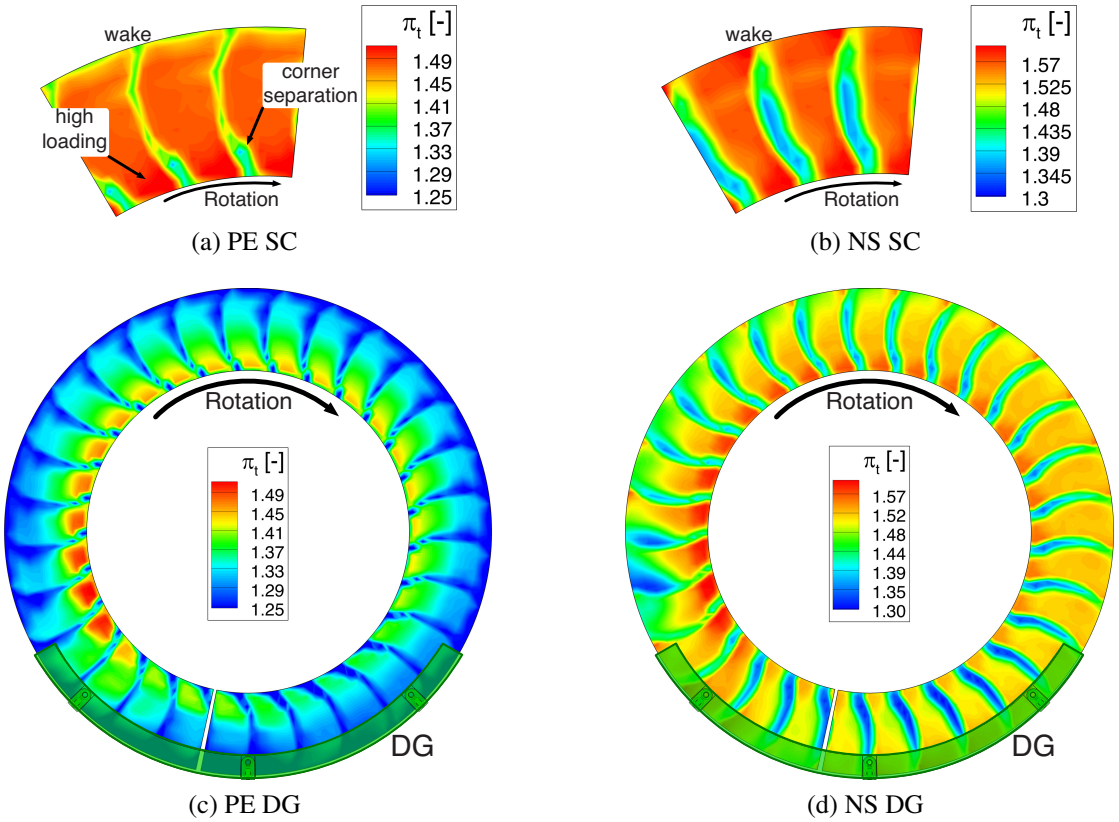

(a) PE SC (b) NS SC

(c) PE DG (d) NS DG

Figure 9: Total pressure ratio at stator exit

Clearly visible for PE in Figure 9a is the quite homogeneous total pressure field with a clear stator wake. A slight gradient is visible in the radial direction. The maximum total pressure ratio is reached at the hub. Close to the stator's wake at the hub a small corner separation appears. When approaching the stability limit (Figure 9b) this changes. The stator wake is strengthened whereas the radial gradient nearly disappears. This is a result of the increased turning of the rotor and the changed loading in the spanwise direction. The turning is increased and therefore the loading of the stator leading to a stronger wake. Throttling the compressor increases the load on the blade tip, which diminishes the radial gradient in the total pressure ratio.

Figures 9c and 9d show the total pressure of the DG configuration. The differences between SC and DG depend on the operating point. At PE, the radial gradient of the total pressure is intensified. Over the whole circumference, the flow pattern and the levels of the reference are not restored. At NS, the wake of the stator changes the position of its maximum depending on the circumferential position. From the entry side, up to around half of the beam, the minimum total pressure is located

at the hub. The wake is intense compared to the rest of the circumference. From the middle of the beam to the exit side, the stator wake is weakened. When the rotor has left the DG, a significant drop in total pressure appears at the casing. This is in accordance with the results from the FHP. As shown in Figure 3, the interaction of the rotor with the separation line shear layer at the exit side is causing this loss. This is seen in the tip flow in Figure 6.

At the entry side of the distortion the incidence of the rotor is lowered, as described above. Therefore the total pressure ratio is lowered. Even though the distortion is only located at the casing, the total pressure ratio changes over the whole radius, which is in agreement with the rotor tip flow shown in Figure 6b. This could be a result of the redistribution of mass flow caused by the blockage of the beam. Inside the separation, the losses in the rotor seem to increase and therefore the total pressure ratio is decreased. These losses are translated further downstream to the stator. At the exit side of the DG the incidence is raised. This causes an increase in total pressure. For PE in Figure 9c, the increased incidence leads to a maximum in total pressure ratio at the corner of the beam close to the exit side support. This is further supported by Figure 6.

CONCLUSIONS

This publication showed the investigation of a transonic compressor stage with a complex inlet distortion flow. In contrast to previous work, a separation was created as well as a total pressure drop, both of which were ingested into the rotor. The flow field in the stage was measured with steady and unsteady techniques. Based on the measurement data a flow model was developed that shows the relevant features.

The main findings are:

1. The pressure field of the separation is complex. Several distinct areas can be defined.
2. The separation is narrowed by the compressor and is influenced by rotation and the shock system.
3. Due to the DG, a swirl component of the flow at the sides of the beam is induced. This swirl leads to a change in incidence, depending on the side of the DG.
4. Operated at the stability limit, the blade tip is not able to recover from the separation and the turbulence is changed around the whole circumference.
5. A loss core is formed by the interaction of the rotor with the separation boundary at the exit side. This loss becomes dominant at NS.
6. The global behaviour of the compressor is changed around the whole circumference and the entire radius.

Additional unsteady data on the behaviour of the compressor at stall onset is available. Circumferentially distributed pressure transducers measured the flow while the rotor was back-pressured until stall. This data will be published and will reveal information on the stall inception process of the rotor with the DG installed.

Data with a high level of detail is delivered that can be used for numerical validation purposes. The change of the flow between PE and NS is complex and very demanding to the numerically model. The data can be used to verify whether a separation in the intake endangers the operation of the engine.

ACKNOWLEDGEMENTS

The members of the FOR 1066 research group gratefully acknowledge the support of the “Deutsche Forschungsgemeinschaft DFG” (German Research Foundation), which funded this research.

REFERENCES

J. Bergner, M. Kinzel, and H.-P. Schiffer. Short length-scale rotating stall inception in a transonic axial compressor - experimental investigation. *Proceedings of ASME Turbo Expo 2006*, GT2006-90209, 2006.

C. Biela, M. W. Müller, H.-P. Schiffer, and C. Zscherp. Unsteady pressure measurement in a single stage axial transonic compressor near the stability limit. *Proceedings of ASME Turbo Expo 2008: Power for Land, Sea and Air; GT2008*, GT2008-50245, 2008.

C. Brandstetter, M. Kegalj, C. Biela, and H.-P. Schiffer. Piv-measurements in a transonic compressor test rig with variable inlet guide vane. *Proceedings of Int. Symposium of Air Breathing Engines 2011*, ISABE-2011-1222, September 2011.

Y. Colin, B. Aupoix, J. F. Boussuge, and P. Chanez. Numerical simulation of the distortion generated by crosswind inlet flows. *18th ISABE 2007*, ISABE-2007-1210, 2007.

M. Davis, A. Hale, and D. Beale. An argument for enhancement of the current inlet distortion ground test practice for aircraft gas turbine engines. *Journal of Tur*, Vol. 124:235 – 241, April 2002.

E. J. Gunn, S. E. Tooze, C. A. Hall, and Y. Colin. An experimental study of loss sources in a fan operating with continuous inlet stagnation pressure distortion. *Journal of Turbomachinery*, Vol. 135, June 2013.

C. A. Hall and T. P. Hynes. Measurements of intake separation hysteresis in a model fan and nacelle rig. *Journal of Propulsion and Power*, Vol. 22, No.4:872 – 879, 2006.

J. A. Lieser, C. Biela, C. T. Pixberg, H.-P. Schiffer, S. Schulze, A. Lesser, C. Kähler, and R. Niehuis. Compressor rig test with distorted inflow using distortion generators. *60. Deutscher Luft- und Raumfahrtkongress*, DGLRK2011-241449:1507 – 1516, September 2011.

F. Lin, M. Li, and J. Chen. Long-to-short length scale transition: A stall inception phenomen in an axial compressor with inlet distortion. *Proceedings of ASME Turbo Expo 2005*, GT2005-68656, June 2005.

J. P. Longley and E. M. Greitzer. Inlet distortion effects in aircraft propulsion system integration. *Steady and Transient Performance Prediction of Gas Turbine Engines*, AGARD Lecture Series 183, 1992.

N. Mishra, D. MacManus, and J. Murphy. Intake ground vortex characteristics. *Proceedings of the Institution of Mechanical Engineers*, Vol. 000 Part G, December 2011.

M. W. Müller. Untersuchungen zum Einfluss von Gehäusestrukturierungen auf die Stabilität und die Leistungsdaten eines transsonischen Axialverdichters. *Dissertation TU Darmstadt*, 2011.

R. Niehuis, A. Lesser, A. Probst, R. Radespiel, S. Schulze, C. Kähler, F. Spiering, N. Kroll, F. Wartzek, and H. Schiffer. Simulation of nacelle stall and engine response. *21st ISABE Conference 2013*, ISABE-2013-10135, September 2013.

R. Radespiel, D. Francois, D. Hoppmann, S. Klein, P. Scholz, K. Wawrzinek, T. Lutz, T. Auerswald, J. Bange, C. Knigge, S. Raasch, P. Kelleners, R. Heinrich, S. Reuß, A. Probst, and T. Knopp. Simulation of wing stall. *43rd AIAA Fluid Dynamics Conference*, 2013-3175, June 2013.

G. Schulze, C. Blaha, D. K. Hennecke, and J. M. Henne. The performance of a new axial single stage transonic compressor. *Proceedings of Int. Symposium of Air Breathing Engines 1995*, 1995.

A. Shmilovich and Y. Yadlin. Engine ground vortex control. *24th Applied Aerodynamics Conference*, AIAA 2006-3006, June 2006.

F. Wartzek, C. Biela, C. Pixberg, and Schiffer, H.-P. Modification of a compressor test rig for measuring the influence of inlet distortions on the compressor flow. *Third Symposium "Simulation of Wing and Nacelle Stall" Braunschweig*, 2012.

F. Wartzek, F. Holzinger, C. Brandstetter, and H.-P. Schiffer. Realistic inlet distortion patterns interacting with a transonic compressor stage. *Fourth Symposium "Simulation of Wing and Nacelle Stall" Braunschweig*, to be published at Springer, 2014.